LA-UR-98-2380

Approved for public release; distribution is unlimited.

Title: COMPARISON OF BAYESIAN AND CLASSICAL RECONSTRUCTIONS OF TOMOGRAPHIC GAMMA SCANNING FOR ASSAY OF NUCLEAR MATERIALS

Author(s): Thomas L. Burr
David J. Mercer
Thomas H. Prettyman

Submitted to:

Los Alamos
NATIONAL LABORATORY

DISCLAIMER

DISCLAIMER

Portions of this document may be illegible in electronic image products. Images are produced from the best available original document.

Comparison of Bayesian and Classical Reconstructions of Tomographic Gamma Scanning for Assay of Nuclear Materials

Tom L. Burr, David J. Mercer, Thomas H. Prettyman
Los Alamos National Laboratory, Los Alamos NM, 87545

Key Words: tomographic gamma scanning, mean squared error of total mass estimate, markov chain monte carlo, errors in variables

1. Abstract

Tomographic gamma scanning has been used to assay special nuclear material for the past several years. Field experience suggests that the data analysis techniques can significantly affect the assay uncertainty. For example, a positive bias has been observed for low-activity samples. Recent attempts to reduce the bias without unacceptable increase in variance have taken a non-Bayesian approach. This paper will compare some of these non-Bayesian approaches to a Bayesian approach which is a modification of an approach used in photon emission computed tomography [1]. The Bayesian approach is both more computationally demanding and more satisfying, though the choice of the prior probability for the distribution of nuclear material can impact the analysis. Assay results for scaled-down versions of the full-dimensioned problem will be presented for several methods and cases.

2. Introduction

Tomographic Gamma Scanning (TGS) is a γ-ray nondestructive assay (NDA) method to assay special nuclear material (SNM) in heterogeneous samples, particularly residues and waste. The principle of the method is that the rate of γ-ray emission is roughly proportional to the total SNM mass T. However, sample-specific attention of the γ-rays complicates the relation between the γ-ray emission rate and T. Furthermore, because the samples could be heterogeneous, both the γ-ray attenuation and source rate vary within the volume of the sample. Therefore, TGS uses tomography to form 3-dimensional images of the γ-ray attenuation. In effect, the attenuation coefficient is estimated in each of many small volume elements (voxels) of the sample. An isotopic transmission source that emits more than one γ-ray (usually Se^{75}) is used to obtain attenuation images as a function of energy. The emission images are then corrected for the attenuation of γ-rays by using the linear attenuation coefficient images. The amount of radioactivity, or the mass if desired, in any region of interest in the sample can then be estimated by integrating the transmission-corrected emission image over the volume of the region. In this paper, the region of interest is the entire sample. The goal is to study the performance of candidate analysis methods in estimating total mass T. See [2] and [3] for more details and caveats about where TGS is applicable.

3. TGS Image Reconstruction

The volume of a 55-gal drum is typically divided into $N = 1600$ 3-dimensional voxels. In a standard scan protocol, data is collected at 150 individual points in polar coordinate (displacement-angle) space for each of 16 vertical layers, giving a total of $M = 2400$ measurement positions (bins) [3]. During an initial scan, transmission measurements are made using an external Se^{75} source to characterize the γ-ray attenuation of the drum. This allows reconstruction (estimation) of the so-called system matrix $A^{M\times N}$. Because of interactions that affect γ-ray energies, the γ count rate at a given energy channel includes the effects of γ's that originated with higher energy but appeared at the given energy channel. The simplest way to account for this underlying background is to measure the (background) γ-rays in energy channels near the channel(s) of interest. The net γ count rate $n = g - c * b$ where g is the observed gross counts in the energy region of interest (ROI) energy channels, b is the observed background counts near the ROI, and c is the ratio of the number of peak ROI channels to the number of background ROI channels. Also, the detection rate of γ-rays must be corrected to a full-energy interaction (FEI) rate that accounts for losses due to deadtime and pulse pileup (detector response issues). The FEI can be estimated by using a Cd^{109} source that emits an 88 keV γ-ray [3], and defined by $FEI = CF(RL) \times n$, where $CF(RL)$ is the estimated correction factor for rate loss. Following [2] we will include $CF(RL)$ in the definition of the $A^{M\times N}$ matrix, which means that when we consider

estimation errors in $A^{M\times N}$, we must include estimation errors in $CF(RL)$. With i indexing bins and j indexing voxels, the image reconstruction problem can then be cast most simply as

$$g_i \sim \text{Poisson}(\sum_j A_{ij}x_j + c\mu_{b,i}), \qquad (1)$$

where x is a vector of nonnegative values that describes the distribution of γ emitting material within the drum, and $\mu_{b,i}$ is the true background count rate from bin i. The observed background counts b_i are well modeled by a Poisson($\mu_{b,i}$) distribution. For our purposes here we can assume that $T = \sum_{i=1}^N x_i$ is the mass of sample. Therefore, our problem is to estimate total mass $T = \sum_{i=1}^N x_i$.

4. Statistical Issues

We assume that $M > N$ in Eq. (1) so ordinary least squares (OLS), or weighted least squares (WLS) are options for estimating each x_i and therefore also T. In fact, Eq. (1) is essentially the same as what commonly appears in a typical 2-stage calibration experiment (stage 1 is the equivalent of our "estimate A stage" and stage 2, which concerns us here, uses the estimated A to estimate $T = \sum_{i=1}^M x_i$. The unique features of our application of Eq. (1) are:

1) The dimension of A is very large (M-by-N is approximately 2400-by-1600) and A is ill-conditioned.

2) There can be significant spatial correlation among neighboring x_i. This is the main reason for the introduction of Bayesian methods in image analysis. Further, it is the main reason for the recent popularity of Markov Chain Monte Carlo (MCMC) methods [4]. MCMC methods are useful for interpreting the nonstandard, large dimensional (N dimensional in this case) posterior probability distributions that arise from using nonstandard prior probability distributions for x^N.

3) The error structure of the *net* response is nonstandard, being $n \sim \text{Poisson}(\mu_g) - c \times \text{Poisson}(\mu_b)$. When g is small, it might be important to use the Poisson distribution rather than an approximating Gaussian.

4) There can sometimes be non-negligible errors in the A matrix. One TGS system [3] deliberately collapses some bins to reduce variance at the expense of slightly increased bias. The usual bias-variance tradeoff suggests that this is a good idea. To date we have ignored the possibility of bias in the A matrix. That is, our errors in A are all modeled as random errors (with standard deviation denoted σ_A here) so future work must include both (1) treatment of possible bias in some entries of the A matrix, and (2) a plan for dealing with dynamically changing dimension of the A matrix due to bin collapsing.

We define our performance measure, $PM_1 = E\{\hat{T} - T\}^2$, where E is the expected value with respect to the distribution of $\hat{T}$. A more typical performance measure in multivariate calibration is $PM_2 = E\{\sum_{i=1}^N (\hat{x}_i - x_i)^2\}$. Note that $PM_1 = E\{[\sum_{i=1}^N (\hat{x}_i - x_i)]^2\}$, so that covariances among the $\hat{x_i}$ can potentially degrade or improve performance, depending on their sign. Very few image analyses are concerned with this particular global performance measure (image analyses tend to try to "sharpen features" or detect edges). It is well known that there is guaranteed to be a biased solution vector $\hat{x}$ that has lower (better) PM_2 than does the OLS solution vector $\hat{x}$ [5]. We expect there is a similar result for PM_1 but we are unaware of it.

Space does not permit us to review all the estimation methods we have implemented and tested on scaled-down versions of Eq. (1) (using $M = 8$ to 100 and $N = 6$ to 50). But we will group them into 5 categories:

A) Methods such as OLS or WLS that do not take explicit account of the Poisson(g) $- c \times$ Poisson(μ_b) error structure and are concerned only with minimizing the sum of squared residuals subject to $\sum_i^M R_i = 0$ (OLS, and more generally WLS, give the minimum variance unbiased residuals [5]).

B) Methods such as the generalized linear model (GLM) which do take explicit account of the Poisson error structure structure. Our GLM implementation assumes that $\mu_{b,i}$ is known and equal to b_i. An "empirical Bayes" argument could justify using $\hat{\mu}_{b,i} = \alpha b_i + (1-\alpha)\bar{b})$ where the weight α could be selected according to the relative variances of the prior and likelihood. But, to date we have only used $\hat{\mu}_{b,i} = b_i$ (which [2] calls the MLEM-FB (fixed background) method) for all of our methods except for MLEM. MLEM jointly estimates μ_b and μ_g by maximizing their joint likelihood.

C) Methods that make some prior assumptions about the magnitudes of the x entries. For example, ridge regression [5] implicitly makes such assumptions and thereby has a Bayesian justification.

D) Methods that make prior assumptions about both the magnitudes of the x entries and their spatial correlation.

E) Methods that consider errors in the A matrix (error in variables (EIV) methods [6]).

Many of our methods can enforce the $x_i \geq 0$ constraint in various ways. The OLS estimates of x_i can be negative, so the simplest approach (which we use)

is to use $\max(0, x_i)$ to enforce the nonnegativity constraint. Elsewhere [7] we report results for methods that both do and do not enforce the nonnegativity constraint.

The methods that work with either the Poisson probability structure (MLEM) of the observed data or that plus a prior probability for each x_i on $(0, C)$ for some large upper limit C (Bayesian methods) deal most naturally with the nonnegativity constraint. For example, we can modify Eq. (1) in [1] to work with g so that the joint probability of g given x, A, μ_b, and c is

$$p(g|x) = \prod_i \frac{\exp(-\mu_{g,i})\mu_{g,i}^{g_i}}{g_i!}, \qquad (2)$$

where $\mu_{g,i} = \sum_j A_{ij}x_j + c\mu_{b,i}$ is the mean of the gross counts at bin i due to all voxels. Reference [8] presented a way to view the transition from maximizing the likelihood in Eq. (2) to maximizing a suitable posterior probability for x that involved a temporary assumption that we could see the contribution at bin i from each individual voxel j. Note however that the mean for g_i at bin i is generally affected by more than one voxel j.

For our Bayesian analysis, we need to specify a prior probability for x. The prior for x in [8] (with the constants c_1 and c_2 absorbed in the definitions of β and δ) is

$$p(x|\beta, \delta) \propto \exp\{-\beta \sum_{i\sim j} \omega_{i,j} \log\cosh(\frac{(x_i - x_j)}{\delta})\}, \qquad (3)$$

and the prior for x in [1] is

$$p(x|\beta, \delta) \propto \exp\{-\epsilon\delta^2 \sum_j x_j^2 - \beta(1+\beta) \times \sum_{i\sim j} \omega_{i,j} \log\cosh(\frac{\delta(x_i - x_j)}{\beta})\}, \qquad (4)$$

where ϵ is a small positive constant (used in [1] to make the prior integrate to 1), $i \sim j$ indicates that the summation is over pairs of "neighbors" (only directly or diagonally adjacent voxels will be assumed to be neighbors), and $\omega_{i,j}$ is a weight that codes the strength of the neighborliness between voxels i and j. We use $\omega_{i,j} = 1$ if i, j are orthogonal nearest neighbors, $\omega_{i,j} = \sqrt{1/2}$ if i, j are diagonal nearest neighbors, and $\omega_{i,j} = 0$ otherwise.

If the constants δ and β in the prior for x are assumed known, then we have essentially the approach in [8]. If the constants δ and β are estimated from the data, then we use a hyperprior ($\Gamma(r_\delta, s_\delta)$, $\Gamma(r_\beta, s_\beta)$ for δ and β, respectively, following [1]). We need to make a minor modification to accommodate the presence of $c\mu_{b,i}$ in either case. While it is more satisfying to try to estimate δ and β from the data (empirical Bayes), it is also more computationally challenging. We have implemented both Eqs (3) and (4). Using (4), we follow [1] and resort to MCMC to generate observations from the posterior of x. The most challenging obstacle to date for us has been to implement the reverse logistic regression method outlined in [1] to estimate the normalization constants for Eq. (4) over a grid of β values. Often with MCMC we can work with unnormalized priors, but in this case, because we use a hyperprior for β, the MCMC updates require the ratio of normalization constants for various β values.

There are always technical issues involving the use of MCMC [4] which must be considered (for example, rate of convergence, proposal distribution parameters, and required chain length). See the appendix of [1] for MCMC convergence issues in our setting. To date, we have used only an informal method to show that the Markov chain does converge to the correct posterior distribution. We simply use different starting values for x, β, and δ, and check that the estimated posterior distribution is insensitive to the starting values. More complete diagnostic tests will eventually be required if this particular Bayes method is implemented in the actual TGS system. Assuming we do generate observations from the posterior distribution for x, these observations can be averaged to give a good estimate of x. Alternatively, when we use Eq. (3), we use the much faster "one step late" (OSL) method from [8] which appears to converge (no proof yet available) to the maximum of the posterior distribution for x.

5. Simulation Study

Elsewhere [7] we report simulated assay results of several classical and Bayesian methods for a 2^6 full factorial experimental design varying the following six factors with $N = 6$ (using values that agree reasonably well with those of real containers except that we use very small M):

(1) condition of A (High or Low),
(2) $M = 8$ or 16,
(3) $\sigma_A = 0$ or $\approx 0.2 \times A$,
(4) $\sum_{i=1}^N x_i = 1$ or 10,
(5) $\sigma_x = 0$ or > 0, (σ_x^2 is the variance of the x_i) and
(6) noise to signal ratio, $\frac{c\mu_b}{Ax} = .2$ or 1.

6. Simulation Results

Here we give assay results for simulated data for a 2^5 full factorial using only the $M = 8$ cases from the the 2^6 full factorial from [7]. Because $\sum(A^TA)^{-1} \approx 38,000$ for cond(A) = H, all the "matrix-inversion" based methods (OLS, WLS, RR, EIV for example) performed badly for cond(A) = H (as expected from classical theory). However, MLEM did remarkably well with only occasional large PM_1 values. The cond(A) = L cases had $\sum(A^TA)^{-1} \approx 5$, so they are expected to do far better than the cond(A)= H cases.

Both Green's OSL and Weir's empirical Bayes methods had to be modified slightly to accommodate the $c\mu_b$ term. We have also used a Bayesian analysis as outlined in [9], and the GLM modeling function in S-Plus. Generally, the Bayesian analysis we implemented based on results in [9] (for the distribution of net counts n assuming a nearly flat Gamma prior for μ_g and μ_b) is slower to implement and has not performed any better than WLS. And, we have had poor results with GLM in S-plus so we will not report those results here.

In Table 1 we present the estimated $PM_1 = E\{\hat{T} - T\}^2$ values for OLS, WLS, RR, MLEM, MLEM-FB, OSL, and EB for for cases 1−32 of a full 2^5 factorial design from [7], varying first the condition of A, then the error variance of A, then T, then σ_x, and finally NSR. That is, run 1 is LLLLL for the 5 factors, run 2 is HLLLL, run 3 is LHLLL, run4 is HHLLL, ..., and run 32 is HHHHH. Table entries are based on 100 simulations per run, so generally, reported PM_1 values are within approximately 20% of their true values.

For OSL, we tried (β, δ) values of $\{(.2, .02), (.02, .002), (2, .002), (.02, .2), (2, .2)\}$. These values were determined by simulation experiments designed to make the OSL give reasonable values. That is, we "calibrated" Eq. (3) for a few known cases and it does appear ([1]) that good $\{\beta, \delta\}$ values depend mainly on the number of voxels N.

An advantage of EB is that is can estimate good values for $\{\beta, \delta\}$. The EB method estimated "good values" for $\{\beta, \delta\}$ to be approximately 0.2 for β and 0.1 to 0.9 for δ, depending mostly on N. Our OSL results were not terribly sensitive to variations in $\{\beta, \delta\}$ within these ranges, so here we report results for "middle values" of $\{\beta, \delta\} = (.2, .02)$.

Concerning the large PM_1 values (1000 or higher) in Table 1, we have observed two types of erratic behavior. First, for MLEM and MLEM-FB, some of the sets of 100 runs had one or two large outliers that dramatically affected the estimated PM_1. We suspect this is due to division by small numbers in the MLEM method. This can also lead to poor starting values for the Bayes methods (because we use the MLEM results as starting values in the Bayes methods). Second, some of the runs had large random variance, as is expected in the classical "matrix-inversion" based methods. Because of the occasional outlier that we do not yet have an explanation for, it is safest to report median values (Fig. 1) of PM_1 to compare methods.

Table 1: Median of $PM_1 = E\{\hat{T}-T\}^2$ results for 100 simulations per run (e3 entries denote times 10^3).

Run	OLS	WLS	RR	MLEM	FB	OSL	EB
1	3.3	2.7	1.6	0.57	0.34	0.35	0.18
2	31e3	19e3	15e3	0.77	0.53	0.57	0.21
3	2.7	1.7	1.5	0.52	0.3	0.31	0.2
4	34	23	20	0.71	0.59	0.72	0.22
5	31	30	16	6.7	6.9	6.1	17
6	330e3	320e3	150e3	7.9	7.7	7	19
7	39	41	24	5	5.1	4.3	12
8	90	89	36	6.3	7.7	5.5	8.6
9	3.5	3.2	1.6	0.69	0.56	0.57	0.55
10	32e3	21e3	16e3	0.58	0.46	0.45	0.28
11	2.8	1.8	1.2	0.52	0.41	0.44	0.33
12	16	7.5	7.7	0.66	0.6	0.59	0.31
13	1.5e3	1.3e3	760	240	280	130	32
14	330e3	330e3	160e3	7.5	7.6	7	6.4
15	290	330	130	49	79	34	24
16	100	89	54	6	6.2	5.6	7.6
17	9.4	8	5.1	0.85	1.3	1.3	1.1
18	59e3	50e3	28e3	1.3	1.8	1.9	0.41
19	200	120	47	9.9	22	17	0.39
20	53	50	30	0.81	1.1	1.2	0.24
21	6.3e3	6.1e3	3.3e3	1.1e3	1.3e3	490	11
22	680e3	650e3	320e3	19	24	17	12
23	64	66	29	10	17	9.6	28
24	200	190	110	15	19	13	14
25	7.5	6.7	3.4	1.3	1.8	1.8	0.46
26	68e3	55e3	29e3	1.1	1.5	1.5	0.33
27	140	110	50	12	24	20	1.8
28	14	11	5.4	1.1	1.3	1.3	0.47
29	99	96	50	16	17	16	90
30	850e3	810e3	400e3	16	22	16	11
31	71	68	39	14	21	15	12
32	400	410	150	16	51	16	12

In Fig. 1a we show the median PM_1 value over all 32 runs for each method. The clear winners are MLEM, MLEM-FB, OSL, and EB.

In Figs. 1b−f we plot the results for the L value followed by results for the H value for each factor for

the seven methods. All L and H values were defined so that we expected smaller PM_1 (better results) for the L value than for the H value. Therefore, the surprises are in Figs. 1b and 1c.

In Fig. 1b, PM_1 is smaller for the H value of the condition of A for MLEM, MLEM-FB, OSL, and EB. Normally we expect worse performance as the condition number of A increases (as we see in Fig. 1b for the OLS, WLS, and RR methods). The L value of condition(A) was approximately 20 (ratio of largest to smallest singular value). The H value of condition(A) was approximately 1300. (This H value is the reason for the very poor performance of all "matrix inversion" based classical methods such as OLS or RR).

In Fig. 1c, we are surprised that increasing σ_A improved the performance of OLS, WLS, and RR (the H value for σ_A gives PM_1 values that are essentially 0 on the scale shown). Perhaps this result is related to our observations that the EIV-based method from [6] did so poorly. When A is both poorly conditioned and measured with error, perhaps it is better to let the errors in A try to shrink the OLS solution toward 0 to mitigate the high variability of $\hat{T}$ that results from A being poorly conditioned.

Also, note that in Figs. 1b and 1c, we report 1/100 times the median of PM_1 for the first three methods (WLS, OSL, and RR). This is simply for plotting purposes so that results from all methods are comparably valued.

The L value of condition(A) was approximately 20 (ratio of largest to smallest singular value). The H value of condition(A) was approximately 1300. (This H value is the reason for the very poor performance of all "matrix inversion" based classical methods such as OLS or RR).

The behavior in Figs. 1c − f is as anticipated in that PM_1 is higher for the H value of the corresponding factor in our experiment. One exception is that EB did as well at the H value for σ_x as for the L value, which is a possible advantage.

It is interesting to see which methods are more sensitive to which factors. We plan to investigate interactions among the five factors in future work.

7. Summary

We have presented a comparison of two Bayesian methods to several "classical" methods. And, we noted that although RR has a Bayesian motivation, there is no attempt to define a neighborhood structure among the xs, so we consider RR to be non-Bayesian in our context. The "best" classical method was MLEM or MLEM-FB, which both performed approximately the same as the two Bayesian methods.

The source of bias in the MLEM method is of interest, as are ways to reduce its bias. Reference [10] presents some methods for reducing bias in maximum likelihood methods. The factors from our list of six candidate factors that actually impact the bias in MLEM are identified in [7]. We believe it will be easier to characterize the bias of MLEM than the bias of any Bayesian method (bias in Bayes methods arises from "incorrect" priors).

Future work will consider the utility of including a probability model for the true A matrix as a way to handle the "errors in variables" aspect to TGS. An additional source of error in A arises from lumpiness of the nuclear material, so current work is aimed at characterizing all error sources in A. However, our initial results suggests that both OSL and the EB methods are not very sensitive to errors in A, so are unlikely to be improved much by treating A as a random variable in a fully Bayesian approach.

The main appeal of an MCMC-based implementation of a Bayesian approach is that we can use the observations from the posterior $p(x|\beta,\delta)$ to estimate the *variability* of $\hat{T}$. So in our case we prefer our EB over OSL because EB gives us more information. This is because the OSL method finds the maximum of the posterior $p(x|\beta,\delta)$, so it cannot be used to estimate the variability of $\hat{T}$.

Estimates of the variability of the MLEM estimator have also been developed [11]. Field studies currently suggest that the actual variability is somewhat smaller than those predicted in [11]. For most applications, we would rather overestimate than underestimate the true variability, so that we tend to be conservative in our claims. Because these variability estimates are available for the MLEM method, an MCMC-based Bayes method is not clearly preferred over MLEM.

We hope to discover through further study whether the ability to estimate β and δ using EB is an important advantage over the simpler OSL method, which must assume a value for both β and δ.

Possibly we will use assumed values for both β and δ to avoid the computational burden of estimating normalization constants, but still use MCMC to generate observations from the posterior $p(x|\beta,\delta)$.

As a result of this study, we believe we can restrict attention to MLEM and MCMC-based Bayesian methods. The main appeal of MCMC-based Bayesian methods is their ability to estimate the variability of $\hat{T}$ while performing reasonably well on PM_1 compared to MLEM.

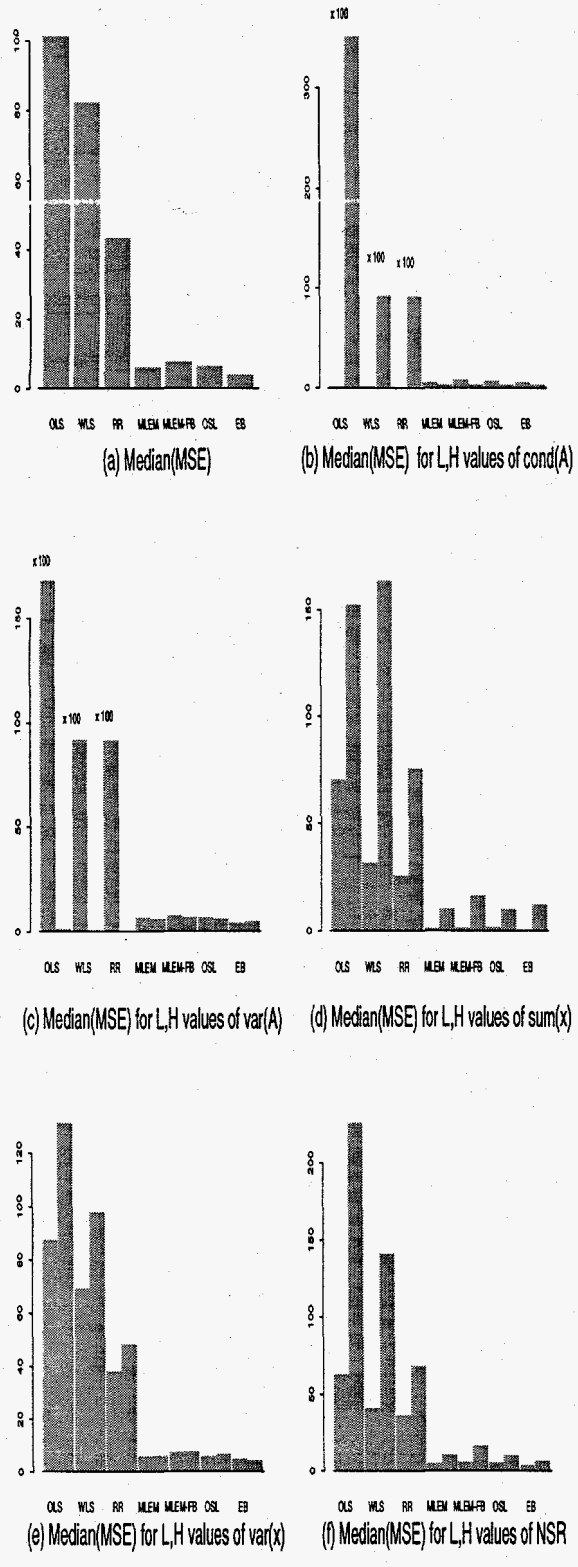

Figure 1: (a) The median of $PM_1 = E\{\hat{T} - T\}^2$ for OLS, WLS, RR, MLEM, MLEM-FB, OSL, and EB. (b-f) Same as (a), but grouped by L and H values of each of the five factors.

8. References

[1] Weir, I. (1997), "Fully Bayesian Reconstructions From Single-Photon Emission Computed Tomography Data," Journal of the American Statistical Association, 92, No. 437, 49-60.

[2] Prettyman, T., Cole, R., Estep, R. and Sheppard, G. (1995), "A Maximum-Likelihood Reconstruction Algorithm for Tomographic Gamma-ray Nondestructive Assay," Nuclear Instruments and Methods in Physics Research A 356, 470-475.

[3] Prettyman, T. and Mercer, D. (1997), "Performance of Analytical Methods for Tomographic Gamma Scanning," LA-UR-97-1168 (Los Alamos National Laboratory document).

[4] Besag, J., Green, P., Higdon, D., and Mengersen, K. (1995), "Bayesian Computation and Stochastic Systems," Statistical Science 10, No. 1, 3-66.

[5] Frank, I., and Friedman, J. (1993), "A Statistical View of Some Chemometrics Regression Tools," Technometrics, 35, No. 2, 109-148.

[6] Fuller, W. (1987), *Measurement Error Models,* Wiley.

[7] Burr, T., Mercer, D. and Prettyman, T. (1998), "A Study of Total Measurement Error in Tomographic Gamma Scanning to Assay Nuclear Material with Emphasis on a Bias Issue for Low-Activity Samples," Proceedings of the 39th annual meeting of the Institute of Nuclear Materials Management, Naples, Florida, July 26-30.

[8] Green, P. (1990), "On Use of the EM Algorithm for Penalized Likelihood Estimation," Journal of the Royal Statistical Society B, 52, No. 3, 443-452.

[9] Mercer, D. Prettyman, T., Abhold, M, and Betts, S. (1997), "Experimental Validation of Tomographic Gamma Scanning for Small Quantities of Special Nuclear Material," Proceedings of the 38th annual meeting of the Institute of Nuclear Materials Management, Phoenix, Arizona, July 20-24.

[10] Kendall, M. and Stuart, A., "The Advanced Theory of Statistics," Volume 2, Griffin and Company (1979).

[11] Prettyman, T. (1995), "Precision Estimates for Tomographic Nondestructive Assay," American Nuclear Society Fifth International Conference on Facility Operations - Safeguards Interface," Jackson Hole, Wyoming, Sept 24-29, LA-UR-95-3299.